



Lawrence Berkeley Laboratory

UNIVERSITY OF CALIFORNIA

RECEIVED
LAWRENCE
BERKELEY LABORATORY

Materials & Molecular Research Division

JUL 24 1984

LIBRARY AND
DOCUMENTS SECTION

Submitted to Wear

EROSION OF CERAMIC THERMAL BARRIER COATINGS

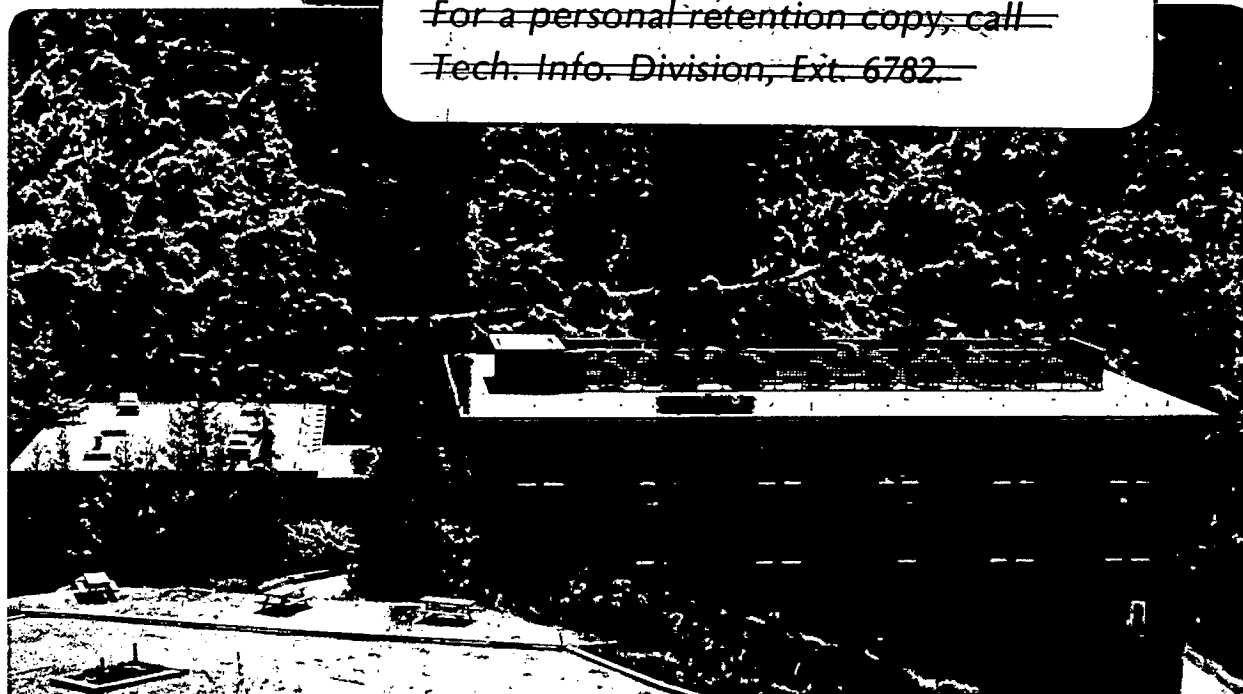
A.G. Davis, D.H. Boone, and A.V. Levy

April 1984

TWO-WEEK LOAN COPY

*This is a Library Circulating Copy
which may be borrowed for two weeks.*

~~For a personal retention copy, call
Tech. Info. Division, Ext. 6782.~~



LBL-15667
c. 2

DISCLAIMER

This document was prepared as an account of work sponsored by the United States Government. While this document is believed to contain correct information, neither the United States Government nor any agency thereof, nor the Regents of the University of California, nor any of their employees, makes any warranty, express or implied, or assumes any legal responsibility for the accuracy, completeness, or usefulness of any information, apparatus, product, or process disclosed, or represents that its use would not infringe privately owned rights. Reference herein to any specific commercial product, process, or service by its trade name, trademark, manufacturer, or otherwise, does not necessarily constitute or imply its endorsement, recommendation, or favoring by the United States Government or any agency thereof, or the Regents of the University of California. The views and opinions of authors expressed herein do not necessarily state or reflect those of the United States Government or any agency thereof or the Regents of the University of California.

LBL-15667

EROSION OF CERAMIC THERMAL BARRIER COATINGS

A. G. Davis, D. H. Boone and A. V. Levy

Materials and Molecular Research Division
Lawrence Berkeley Laboratory
University of California
Berkeley, California 94720

April 1984

This work was supported by the Assistant Secretary of Fossil Energy, Office of Coal Research, Heat Engines and Heat Recovery Division of the U.S. Department of Energy under Contract Number DE-AC03-76SF00098 through the Battelle Memorial Institute, Pacific Northwest Laboratories, Richland, WA.

ABSTRACT

A study has been made to relate the erosion behavior of several experimental zirconia-base ceramic thermal barrier coatings to their processing parameters and microstructure. The incremental erosion rates were measured and each specimen was examined using optical and scanning electron microscopy. Erosion experiments were conducted in a room temperature erosion test apparatus using 63-100 μ m silica erodent particles with impact velocities of 30m/s (\sim 100fps). Erosion rates in the steady state condition are presented for impingement angles of 30 and 90 degrees. It has been determined that significant differences in erosion rates occurred due to processing parameter variations, composition and resulting coating morphology. Initial erosion rates were found to be strongly dependent on surface roughness while steady state erosion appears to be more dependent on intrinsic coating properties and porosity.

INTRODUCTION

General Background

The degradation of ceramic thermal barrier coatings (CTBC) from exposure to erosive environments is of practical and economic importance to the designers of diesel and gas turbine engines. The demand for greater durability and fuel versatility in engines has stimulated development of thermally insulated combustion zone components that operate in a higher range of temperatures and in overall harsher environments than those of current diesel engines and stationary gas turbines. Thermal protection of combustion chamber components can be achieved through the use of ceramic thermal barrier

coatings. Oxide ceramic coatings, however, are generally susceptible to greater erosion rates than are the traditional metallic coatings.¹ The presence of small particles such as coal ash, char or minerals within the combustion zone from the use of degraded, synthetic or coal containing fuels produces an erosive environment which can result in accelerated engine component coating failures.

Present Study

Ceramic Thermal barrier coatings (CTBC) have a variety of failure modes.² Of primary concern in state-of-the-art applications are failures caused directly by thermal fatigue, two and three-body wear and erosion. Traditionally, trade-offs between improvements in wear behavior and thermal fatigue behavior have often been required. Processing controls designed to improve thermal fatigue resistance such as increasing porosity, use of mixed phases and partially stabilized phases, and introducing segmentation with microcracking may have detrimental effects on a coating's erosion resistance. Recent developments in processing and structural control have been aimed at mitigating some of these effects.

Fully and partially stabilized zirconia has proven itself as an effective thermal barrier and a successful coating system in many current applications. Determining the baseline, room temperature erosion behavior of specimens coated with partially stabilized zirconia base coatings is important as an aid in understanding the relationships between coating variables and erosion behavior, as a basis for comparison of available coating systems and in assessing the need for

protection of the CTBC from erosive environments. The experiments performed were designed not to actually simulate the operating environment of a coated combustion zone component but to determine the relative erosion resistance of certain experimental coating systems as an initial step in the material selection and refinement process.

EXPERIMENTAL

Rectangular specimens 3mm x 19mm x 25mm (1/8' x 3/4' x 1') were secured, coating side up, to the specimen holder of a room temperature erosion testing apparatus.¹ A previously weighed amount of 63-100 μ m SiO₂ erodent particles was placed in the vibrating particle hopper which feeds the particles into a 46cm long, 5mm ID nozzle directed vertically downward at the specimen, shown schematically in Fig 1. A particle velocity of 30m/s (\approx 100fps) was used at impingement angles of 30° and 90°. The impingement angle is easily adjusted by rotating the specimen holder. An adjustable pressure differential introduced across the nozzle establishes the particle velocity which is measured using a rotating disk method.³ During the incremental erosion test periodic specimen weighings were made and plotted against the cumulative erodent weight. This weight loss curve was then graphically differentiated to yield incremental erosion rates. Selected as-received and eroded specimens were prepared for surface analysis using a 0.0001 inch R diamond stylus profilometer and for metallographic examination using optical and scanning electron microscopy (SEM). Cross sections as well as surface micrographs were examined. Plasma spray⁴ and electron beam-physical vapor deposition (EB-PVD)⁵ methods of coating deposition were used.

RESULTS

Descriptions of the coating systems eroded in this study are presented in Table 1. Table 2 lists the average Vickers hardness and the steady state erosion rates of each system for impingement angles of 30° and 90° . The Vickers hardness levels listed represent the average value obtained when measured using 300 grams applied to the coating cross section.

A wide variation in coating morphologies was observed for the zirconia systems examined. Most apparent were visual differences in porosity and initial surface roughness. The CTBCs' thicknesses ranged from 45 to $1100\mu\text{m}$ with average thickness of $450\mu\text{m}$. Metallic bond coats between the substrate metal and the ceramic coating did not differ substantially in composition, appearance or thickness among the plasma sprayed systems. In general, plasma sprayed coatings will be well bonded to properly prepared substrate surfaces,⁶ and, therefore, bond strengths were not considered relevant to this erosion study.

Coating Systems No. 1 and No. 2 are shown in cross section in Figs. 2a and 2b, respectively. System No. 1 ($6.6\text{wt}\% \text{Y}_2\text{O}_3\text{-ZrO}_2$) is seen to have a much less porous CTBC structure than System No. 2 ($6.6\text{wt}\% \text{MgO-ZrO}_2$).⁷ The bond coats were both applied by an air plasma spray technique and are very similar to one another and were therefore not considered to be important when comparing erosion rates of these systems. The surfaces of Systems No. 1 and No. 2 were examined using SEM in both the as-coated and eroded surface conditions. Examination of all eroded surfaces was conducted after steady state erosion was reached. Typical surface conditions are shown for System No. 1 and

System No. 2 in Figs. 3 and 4, respectively.

Fig. 5 presents the incremental erosion rate curves of these systems as plotted against the cumulative erodent weight to indicate system behavior during the transition prior to achieving steady state erosion conditions and to indicate the erosion rate at which steady state conditions are achieved. It can be seen that the steady state erosion rate of the 6.6wt% $Y_2O_3-ZrO_2$ coating ($0.5 \times 10^{-4}g/g$) is less than half that of the 6.6wt% $MgO-ZrO_2$ coating ($1.1 \times 10^{-4}g/g$). The graph also indicates that twice the amount of erodent particles are required to bring the more porous $MgO-ZrO_2$ coating to steady state erosion compared to the $Y_2O_3-ZrO_2$ system. Systems No. 1 and No. 2 exhibited the lowest erosion rates of all of the materials tested (see Table 2).

The 20wt% $Y_2O_3-ZrO_2$ coating of System No. 3 was deposited using an EB-PVD method. Its columnar and surface structures shown in Fig. 6a and 6b differ significantly from the lenticular structures of the plasma sprayed coatings and are in large part responsible for the coating's superior resistance to thermal fatigue.⁸ Previous attempts to improve thermal fatigue resistance often resulted in sacrificing erosion resistance. However the EB-PVD process was included in this study in hopes of identifying potential structural alternatives to such trade-offs. Fig. 6c shows the eroded EB-PVD surface after reaching its steady state erosion rate of $1.2 \times 10^{-4}g/g$ (Table 2).

Surface analyses were performed on system No.3 in the as-coated and eroded conditions and are shown in Fig. 7a and 7b. This was done to facilitate a comparative study of surface roughnesses before and after

erosion.

Coating system Nos. 4, 5 and 6, each with an 8wt% $Y_2O_3-ZrO_2$ partially stabilized thermal barrier coating, are shown in cross section in Fig. 8. Coating composition was maintained as the constant parameter so that erosion rate differences could be attributed to unique physical properties such as apparent porosity, hardness, microcracking and to differences in starting powder and deposition parameters. As quantitative porosity measurements were not made, statements regarding relative porosities are qualitative and based on comparisons made from observations of samples carefully prepared under the same techniques and are therefore referred to as 'apparent' porosities.

Table 2 shows the erosion rates and average Vickers hardness for these three systems. The 30° erosion rates of systems No. 4, No. 5 and No. 6 were reduced approximately 38%, 13% and 6%, respectively, from the 90° rates. It is observed from Table 2 and Fig. 8 that increasing erosion rates correspond to decreasing hardness and to increasing apparent porosities.

Fig. 9 shows the erosion behavior of each of the 8wt% $Y_2O_3-ZrO_2$ systems. The regions of flattening out of the curves represent the point at which the same amount of coating mass is removed for each increment of particle impacts. The point at which this occurs, or the time to reach steady state erosion, can also be attributed to coating morphology. Coating System No. 6 has the greatest degree of apparent porosity and is seen to require approximately 20 grams of erodent to reach the steady state, whereas System No. 4 has a denser structure

allowing steady state to be reached within approximately 12 grams.

Figs. 10 and 11 show Systems No. 4 and No. 6, respectively, in the as-sprayed and eroded conditions. These micrographs give some indication of surface splat size (globule of sprayed material) and degree of microcracking. It has been shown that microcracking has a beneficial effect on fracture strength, thermal shock resistance and possibly impact resistance as well.⁹ Much attention is given in powder and processing selection to obtain increased amounts of controlled micro-cracking. The eroded surfaces show that the coatings' initial, rougher surfaces have smoothed out as the as-deposited peaks are removed by the erosion process. This smoothing tendency is seen more clearly in the surface profiles of system No. 6 in the as-coated (Fig. 12a) and eroded (Fig. 12b) surface conditions. In addition, this system was eroded after the as-coated surface had been polished for 5 minutes using $1\mu\text{m Al}_2\text{O}_3$. This was done to study the effect that as-coated surface protrusions have on the initial erosion rate of CTBC's. The surface profiles of the as-coated, polished and eroded conditions are shown in Fig. 13, while the erosion rate of the polished system has been plotted and is presented in Fig. 14.

Fig. 15 shows the surface of System No. 6 in the (a) as-coated and (b) $\alpha=90^\circ$ eroded conditions under high magnification. Large protrusions can be seen in the as-coated surface that are vulnerable to being knocked off early in the erosion process. During steady state erosion the surface has no large protrusions and is smoother by comparison.

Coating System No. 7 represents still another structural

modification. Its metallic-ceramic inner layer was included in this study for contrast. As seen in Tables 1 and 2, this system's extremely thick thermal barrier coating experienced a very high relative steady state erosion rate. Fig. 16 shows the coating in cross section showing the intermediate layer of a bond alloy and zirconia mixture between the quite porous MgO-ZrO₂ outer layer and the inner bond layer. Erosion measurements at 30° were not made because of limited specimen availability.

DISCUSSION

Determination of baseline erosion behavior at room temperature is a rapid, inexpensive process by which initial comparisons can be made of ceramic thermal barrier coatings (CTBC). Comparing the erosion rates of similar coatings to their physical and chemical properties gives insight into the mechanism by which the coating is eroded. One may then be able to draw initial conclusions as to the effect of process variables on the erosion mechanism and rate. This is of fundamental importance in the task of producing less erosive CTBC's. It may then be possible to combine the knowledge of erosion behavior with that of thermal fatigue behavior to produce better, more durable, commercial CTBCs.

The Effect of Surface Roughness on Initial Erosion Rates

One of the striking observations of the CTBC erosion rate curves is the initially high rate of coating removal and subsequent leveling off to steady state that is common to most all ceramic coatings of the type being studied (Figs. 5 and 9). This is best explained by

comparing as-coated surfaces to the same area after steady state erosion has been reached. Referring to Figs. 10, 11 and 15 it is seen that the initial surface of a plasma sprayed ceramic coating is one which has a rough texture while the eroded surface appears much smoother. The surface profile data of Figs. 7 and 12 supports these observations by showing an average height of protrusion which has been reduced significantly by erosion. Protrusions of the ceramic which have been deposited during the semi-molten deposition process often form a rough and brittle surface. The initial blast of erodent particles against these vulnerable protrusions breaks them off at a very high rate. The new area exposed to erosion is a smoother ceramic surface that has a much greater resistance to erosion. Thus, the initially high erosion rate subsequently decreases to a lower rate of material loss shortly after the original surface is removed. When the steady state rate of material removal is reached it is at a constant, relatively low rate.

Polishing the surface of system No. 6 prior to erosion had the effect of the initial erosion mechanism by smoothing off the ceramic protrusions. In fact, comparison of Fig. 13b with Fig. 12b and 13c shows that the polishing produced a surface which appeared to be smoother than that of the steady state eroded surface. As erosion proceeded, the polished surface became rougher, reaching the same degree of roughness at steady state as the unpolished specimens. Because the surface smoothing had in some part already been performed by the polishing, the initial rate of erosion was lower, as shown by comparison of Figs 14 and 9. Note that the steady state rate of erosion

did not change.

Because of the rapidity with which steady state erosion is achieved, steady state erosion and not initial erosion appears to control coating erosion resistance. The study of initial erosion rates is a significant contributor to understanding CTBC erosion mechanisms.

The Effect of Apparent Porosity on Steady State Erosion in Plasma Sprayed Coatings

As a coating with a relative high degree of apparent porosity erodes, it continually exposes new voids. Although the overall surface roughness decreases until it reaches a minimum at the steady state condition, the newly exposed surface of a porous coating is nevertheless characterized by ceramic protrusions. These vulnerable protrusions behave in a manner similar to those of the as-deposited coating surface and are repeatedly being exposed and removed as erodent particles continually impact them. Because variations in the coating systems of this study extended beyond isolation of the porosity variable, it is difficult to conclude that this type of protrusion mechanism dominates erosion behavior. However comparing the erosion rate data of Table 2 with the photomicrographs of Figs. 2, 8 and 16, one sees a consistent direct relationship between the amount of porosity and the erosion rate.

Systems No. 4 and No. 5, for example, differed only in initial powder deposition temperature, thickness and apparent porosity. The difference in the deposition temperature, controlled by the electric current of the plasma spray gun (Table 1), had the effect of depositing coatings of two distinctly different levels of apparent porosity. The

more dense 900 amp system, No. 4, has a lower rate of erosion than the 600 amp system with the rate difference increasing in significance at the shallower impingement angle of 30° (Table 2). Examining system No. 6, whose composition is the same as systems No. 4 and No. 5, one observes a still greater degree of porosity with a correspondingly higher steady state erosion rate.

Other Effects

It is likely that other effects also influence erosion behavior. Some correlation was seen between coating hardness and erosion rate and between coating structures and erosion rate, as discussed above. Since very little work and data collection in the area of ceramic thermal barrier coating erosion has been published to date, it is difficult to propose a dominant erosion mechanism. Hardness and structure interact with phase composition, microcracking and other properties in a complex manner. More definitive conclusions as to how these properties interact with one another to influence erosion behavior and as to whether a specific property will dominate erosion effects must await a larger collection of experimental data and improved processing controls.

CONCLUSIONS

1. Initial erosion rates of partially stabilized, plasma sprayed, zirconia base ceramic thermal barrier coatings (CTBCs) is directly related to initial surface roughness.
2. The apparent porosity of CTBCs influences erosion directly, with

higher porosity coatings exhibiting higher steady state erosion rates.

3. The electron beam-physical vapor deposition method which produces a columnar structured CTBC exhibits good erosion resistance as well as proven durability in thermal cycling.
4. Hardness and microcracking, while influencing erosion behavior, were not observed to be dominating factors.
5. Adherence at the bond coat-ceramic coat interface is not related to erosion behavior in state-of-the-art plasma sprayed coating systems.

ACKNOWLEDGMENTS:

This work was supported by the Assistant Secretary of Fossil Energy, Office of Coal Research, Heat Engines and Heat Recovery Division of the U.S. Department of Energy under Contract No. DE-AC03-76SF00098 through the Battelle Memorial Institute, Pacific Northwest Laboratories, Richland, WA.

REFERENCES

1. Zambelli, G. and Levy, A. "Particulate Erosion of NiO Scales", Wear Vol 68, No. 3, p 305-332, May 1983.
2. Miller, R.A., Lowell, C.E., "Failure Mechanisms of Thermal Barrier Coatings Exposed to Elevated Temperatures", April 1982. NASA Technical Memorandum 82905.
3. Ruff, W.A., Ives, Wear 35, pp.195-199 (1975).
4. Steffens, H. D. Materials Coating Techniques (NATO Agard Lecture Series No. 106) pp. 5-4 to 5-8, 1980.
5. Demaray, R.E., "Dedicated Electron Beam Reactive Physical Vapor Deposition (R.P.V.D.) Apparatus for the Production of Ceramic Thermal Barrier Coatings", Airco Temescal Division Project Final Report, May 1981. DOE Subcontract No. B-A0760-A-U.
6. Taylor, T. A., Price, M. O., Tucker, R. C., 'Development of Evaluation of Plasma Sprayed MgO-ZrO₃ and ZrO₂-Y₂O₃ Thermal Barrier Coatings,' Union Carbide Coatings Service Project Report No. 100.
7. Anderson, N.P., Ruckle, D. L., "Program for Development of Strain Tolerant Thermal Barrier Coating Systems", August 1981, under NASA contract NSS3-22548.
8. Siebeneck, H. J., Cleveland, J. J., Hasselmann, D. P., Baardt, R.C. "Thermal Diffusivities of Microcracked Polycrystalline Ceramics", Ceramic Microstructures 1976, pp 753-762 (1977).

FIGURES

1. Schematic diagram of the room temperature erosion apparatus.
2. Cross sections, of a) System No. 1 and b) System No. 2 showing differences in the CTBC porosities.
3. System No. 1 surface, in the a) as-coated and b) eroded at 90° conditions.
4. System No. 2 surface in the a) as-coated and b) eroded at 90° conditions.
5. Incremental erosion rate comparison between 6.6wt% $Y_2O_3-ZrO_2$ (System No. 1) and 6.6wt% $MgO-ZrO_2$ (System No. 2) plasma spray coatings.
6. System No. 3, 20wt% $Y_2O_3-ZrO_2$, EB-PVD in the a) as coated substrate- cross section, b) as-coated surface, c) surface after steady state erosion condition.
7. Surface profiles of system No. 3 a) as-coated and b) after steady state erosion. Vertical scale: 1 division = 200 micro-inches, chart speed 0.5 in/sec., traverse speed 0.01 in/sec.
8. As-coated cross sections of the 8 wt% $Y_2O_3-ZrO_2$ systems: a) system No. 6, b) system No. 5 and c) system No. 4.
9. Incremental erosion rates of 8wt% $Y_2O_3-ZrO_2$ coating systems.
10. Surface of System No. 4, a) as-coated, b) eroded at 30° , c) eroded at 90° .
11. System No. 6, a) as-deposited and b) eroded at 90° conditions.
12. Surface profiles of System No. 6, a) as-coated and b) after steady state erosion. Vertical scale: 1 division = 200 micro-inches, chart speed 0.5 in/sec., traverse speed 0.01 in/sec.
13. Surface profiles of system No. 6: a) representative profile of the as-coated surface, b) system surface following a 5 minute polish with 1 μ m alumina, c) profile of polished surface after erosion to the steady state condition. Vertical scale: 1 division = 200 micro-inches, chart speed .5 in/sec., traverse speed 0.01 in/sec.

14. Incremental erosion rate of system No. 6 after the as-coated surface was polished for 5 minutes with $1\mu\text{m Al}_2\text{O}_3$.
15. System No. 6 in the a) as-coated and b) eroded at 90° condition under high magnification.
16. Cross section of system No. 7 showing the mixed region of MgO-ZrO_2 and CCrAlY provided primarily for CTBC adherence enhancement.

Table I
Description of Ceramic Thermal Barrier Coating Systems (CTBC)

Coating Systems	Thermal Barrier Coat (TBC) Composition, Wt.%	CTBC Thickness (μm)	Bond Coat (BC) Composition	BC Thickness (μm)	Thermal Barrier Coat Deposition Method
No. 1	6.6Y ₂ O ₃ - ZrO ₂	350	NiCoCrAlY	155	Plasma Spray with post coating heat treatment
No. 2	6.6MgO - ZrO ₂	350	NiCoCrAlY	155	Plasma Spray with post coating heat treatment
No. 3	20Y ₂ O ₃ - ZrO ₂	45	NiCrAlY	45	Electron Beam - Physical Vapor Deposition (EB-PVD)
No. 4	8Y ₂ O ₃ - ZrO ₂	465	NiCrAlY	115	Plasma Spray at 900 amps
No. 5	8Y ₂ O ₃ - ZrO ₂	310	NiCrAlY	155	Plasma Spray at 600 amps
No. 6	8Y ₂ O ₃ - ZrO ₂	500	NiCoCrAlY	125	Plasma Spray
No. 7	MgO-ZrO ₂	1100	graded	200	Plasma Spray

Table II
Steady State Erosion Rates and Average Vickers Hardness of Thermal Barrier Coating Systems

Coating System	Average Vickers Hardness, HV	Steady State Erosion Rate ($\times 10^{-4}$ g/g)	
		$\alpha=90^\circ$	$\alpha=30^\circ$
No. 1	680	0.5	0.4
No. 2	630	1.1	0.9
No. 3	890	1.2	1.6
No. 4	660	2.1	1.3
No. 5	570	2.3	2.0
No. 6	370	3.6	3.4
No. 7	375	10.0	-

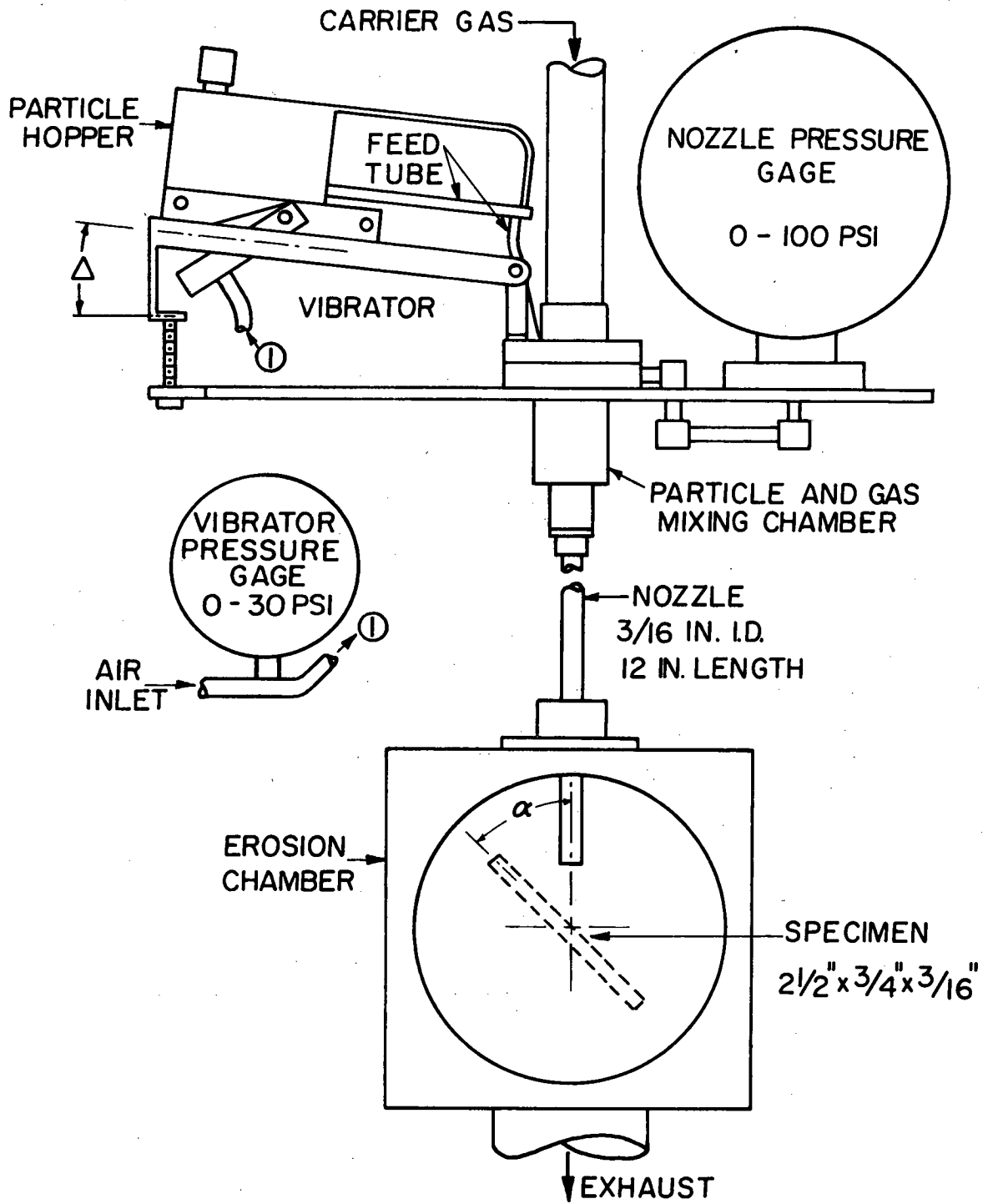
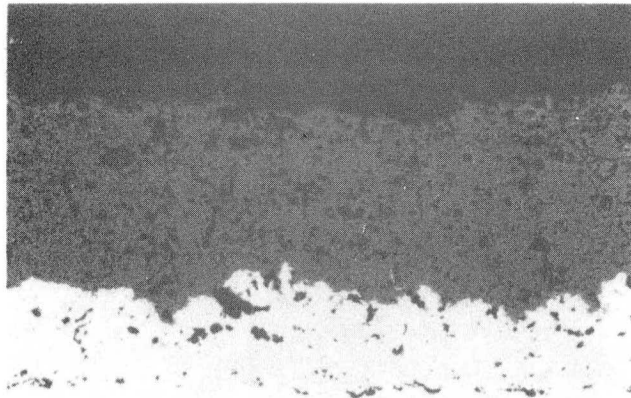


Fig. 1. Schematic diagram of the room temperature erosion apparatus

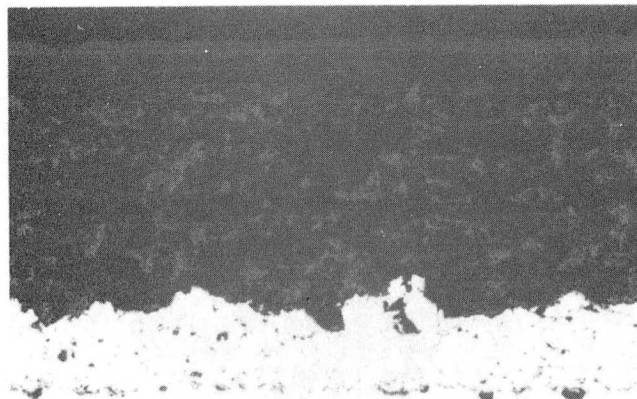
XBL775-5525



a

6.6 w/o YSZ

155 μm



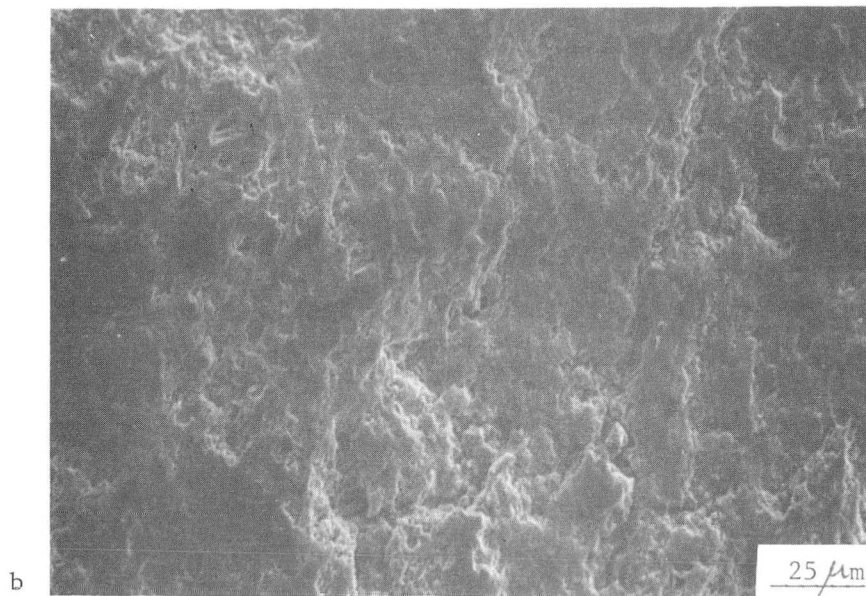
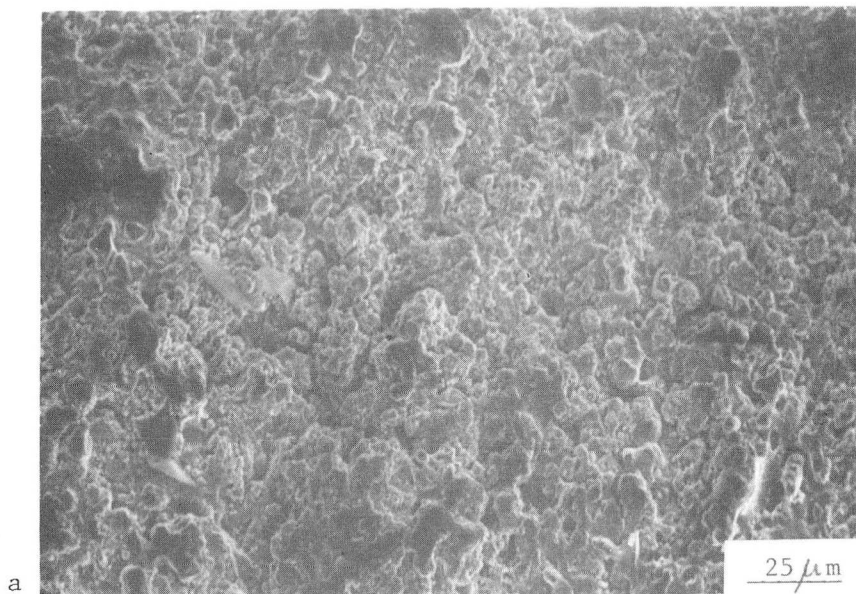
b

6.6 w/o MgSZ

155 μm

XBB 829-7747A

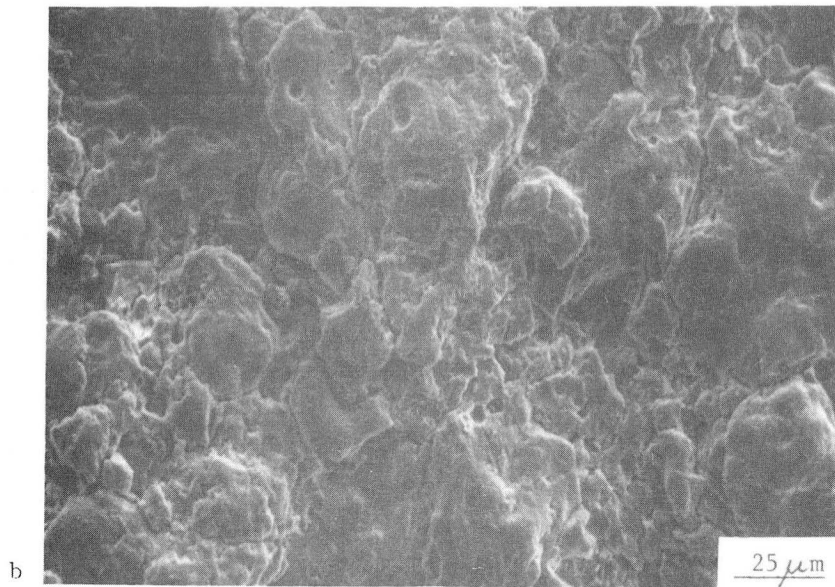
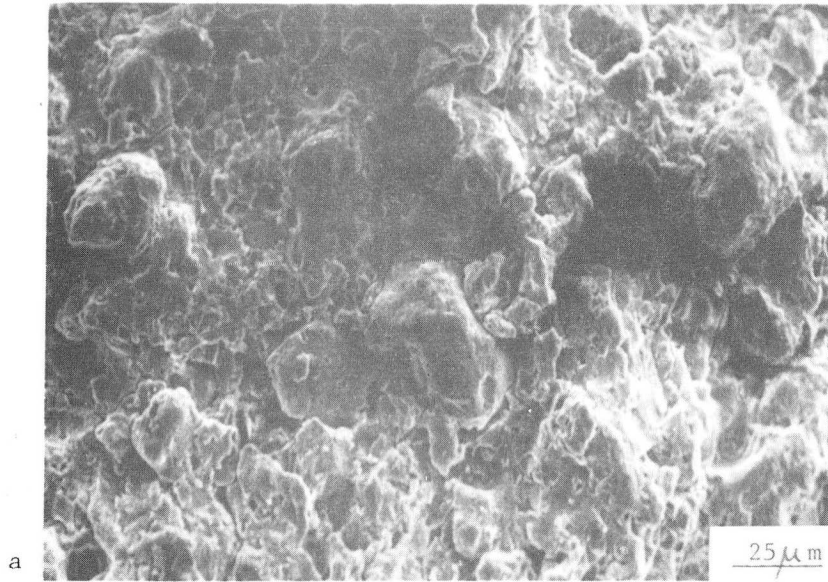
Fig. 2. Cross sections of a) system no. 1 and b) system no. 2 showing differences in the CTBC porosities



XBB 829-7748

Fig. 3. System no. 1 surface in the a) as coated and b) eroded at 90° conditions

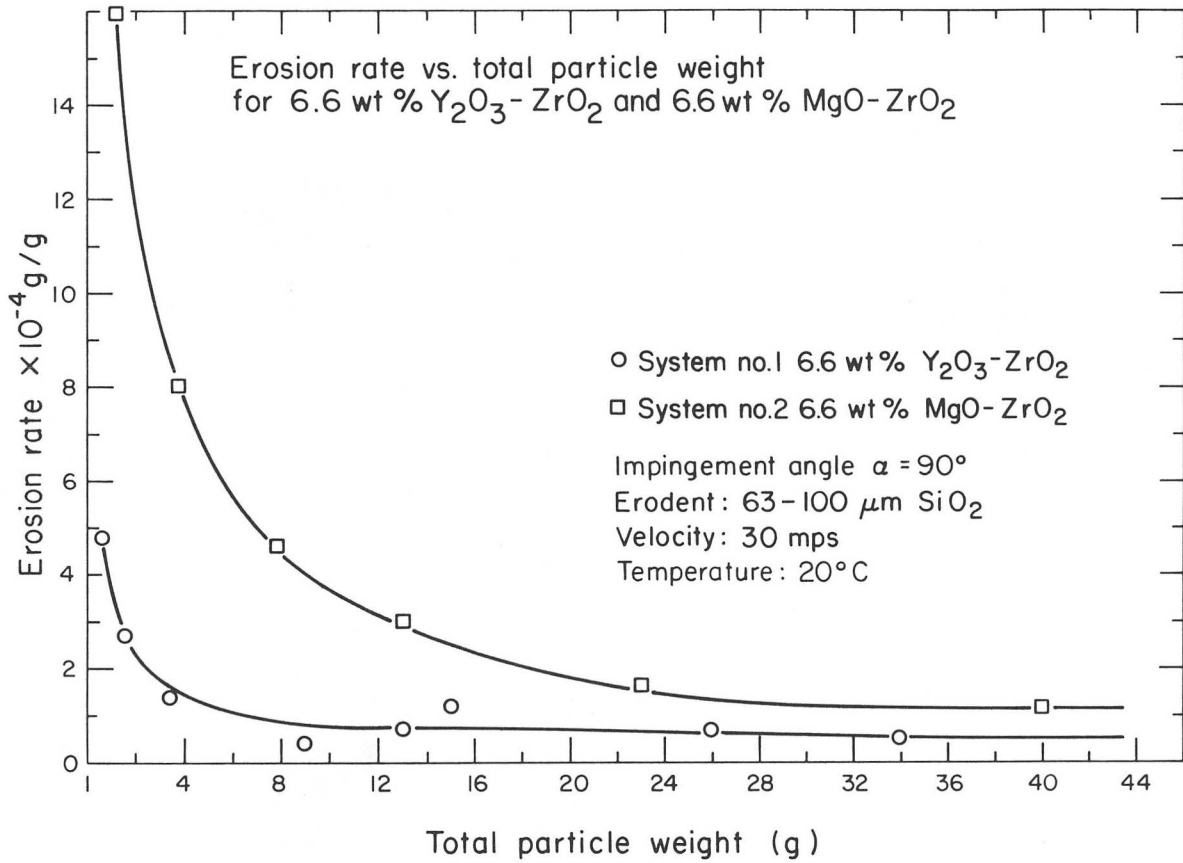
6.6 W/o YSZ



XBB 829-7749

Fig. 4. System no. 2 surface in the
a) as-coated and b) eroded at 90°
conditions

6.6 W/o MgSZ



XBL 829-1130A

Fig. 5. Incremental erosion rate comparison between 6.6 wt% $Y_2O_3-ZrO_2$ (system no. 1) and 6.6 wt% $MgO-ZrO_2$ (system no. 2) plasma spray coatings

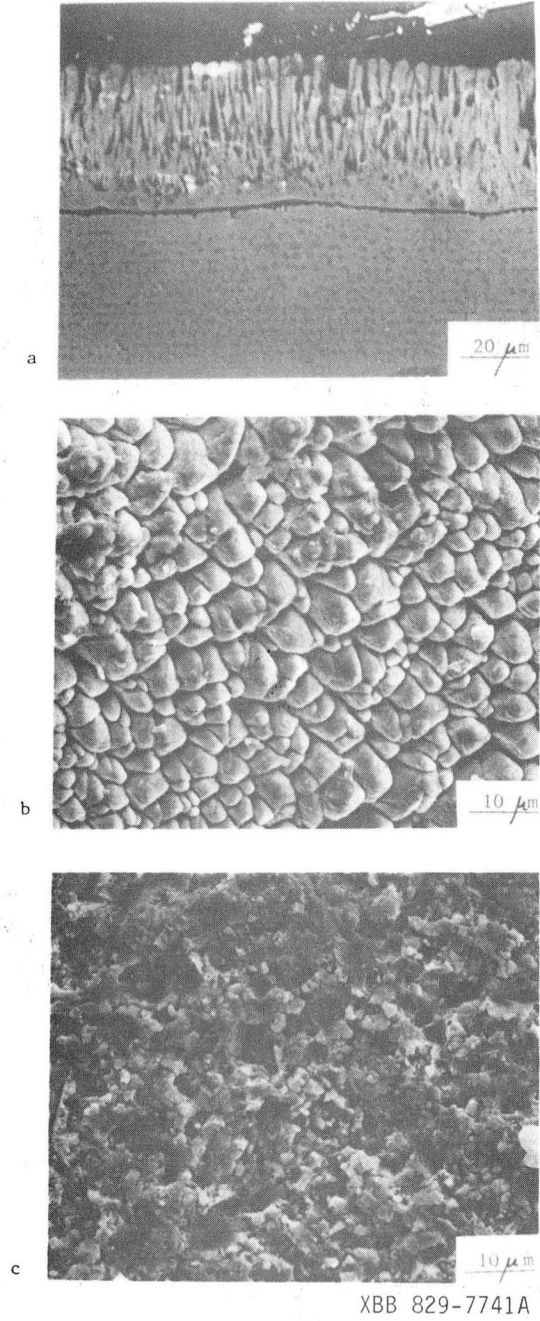
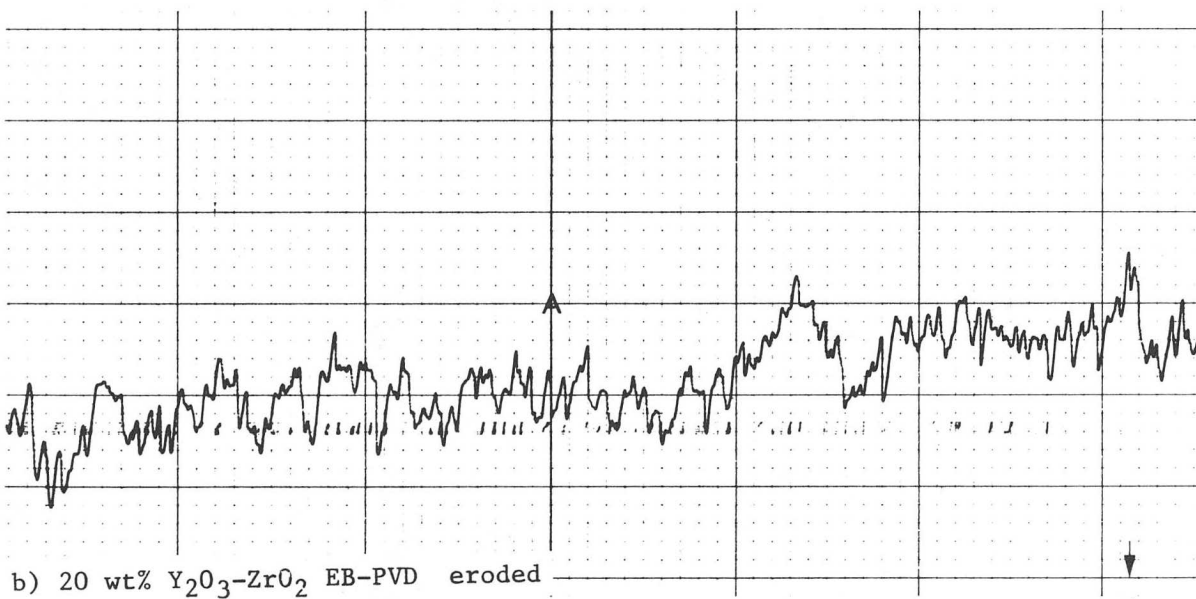
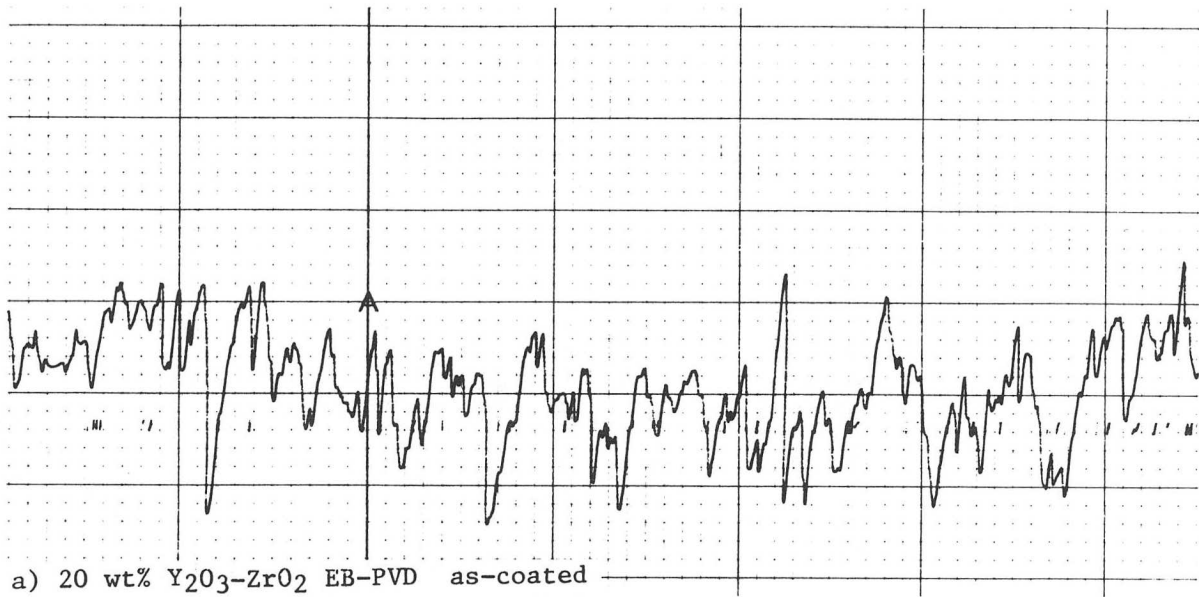


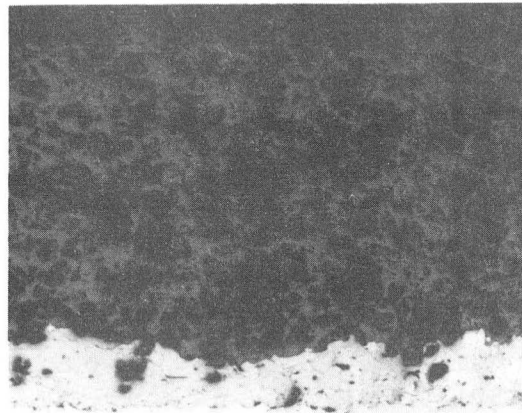
Fig. 6. System no. 3, 20 wt% Y_2O_3 - ZrO_2 EB-PVD, in the a) as-coated substrate-coating cross section, b) as-coated surface and c) surface after steady state erosion conditions



XBL 836-10480

Fig. 7. Surface profiles of system no. 3
 a) as-coated and b) after steady
 state erosion. Vertical scale:
 1 division = 200 micro-inches, chart
 speed 0.5 in/sec., traverse speed
 0.01 in/sec.

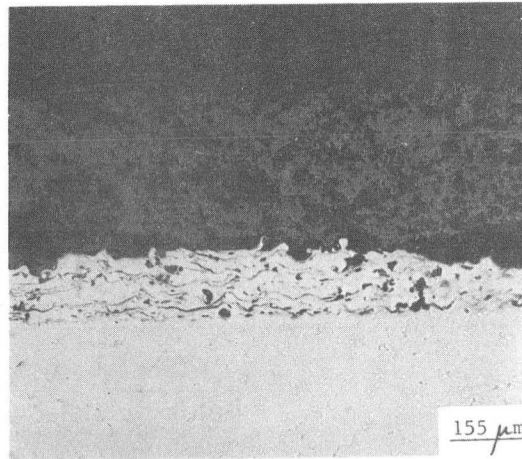
8^{w/o} YSZ



a

125 μm

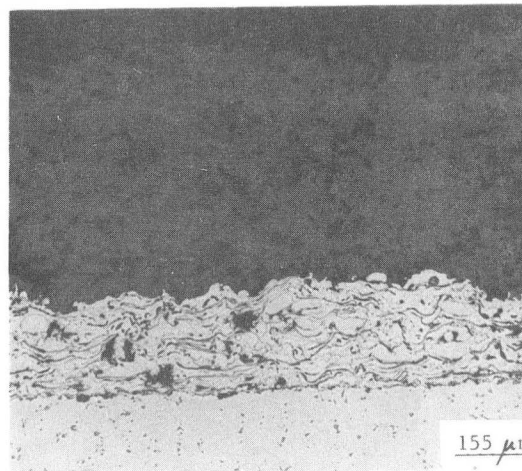
8^{w/o} YSZ 600 amp



b

155 μm

8^{w/o} YSZ 900 amp



c

155 μm

XBB 829-7742

Fig. 8. As-coated cross sections of the 8 wt% $Y_2O_3-ZrO_2$ systems: a) system no. 6
b) system no. 5 and c) system no. 4

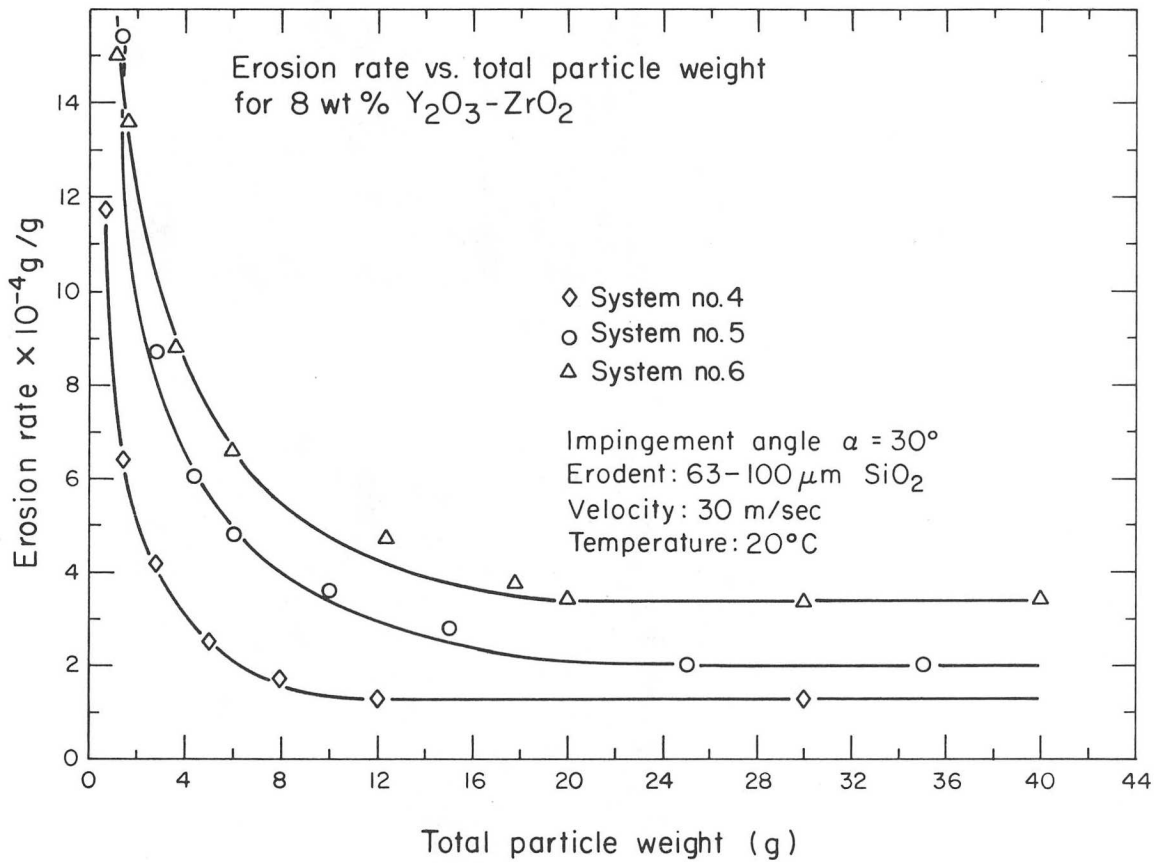
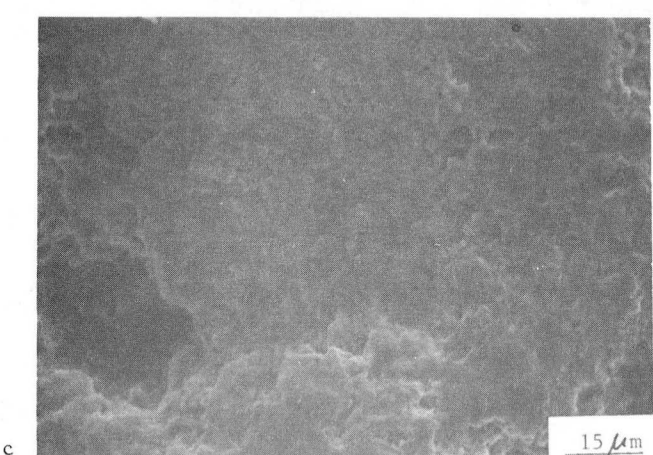
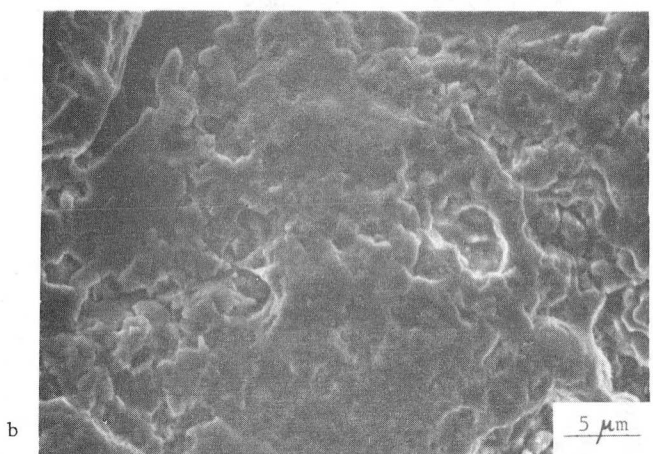
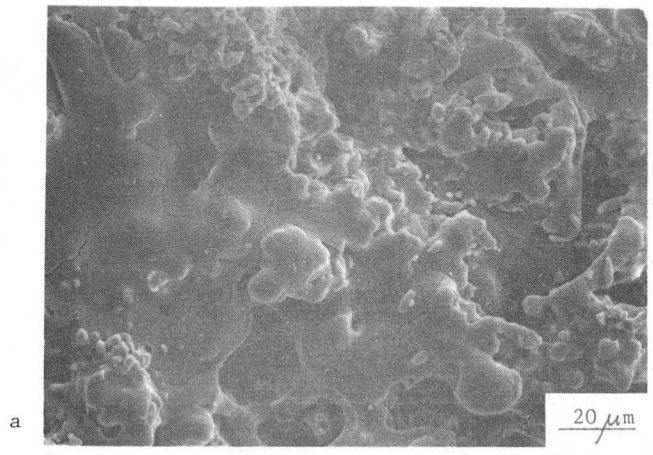


Fig. 9. Incremental erosion rates of 8wt% $Y_2O_3-ZrO_2$ coating systems

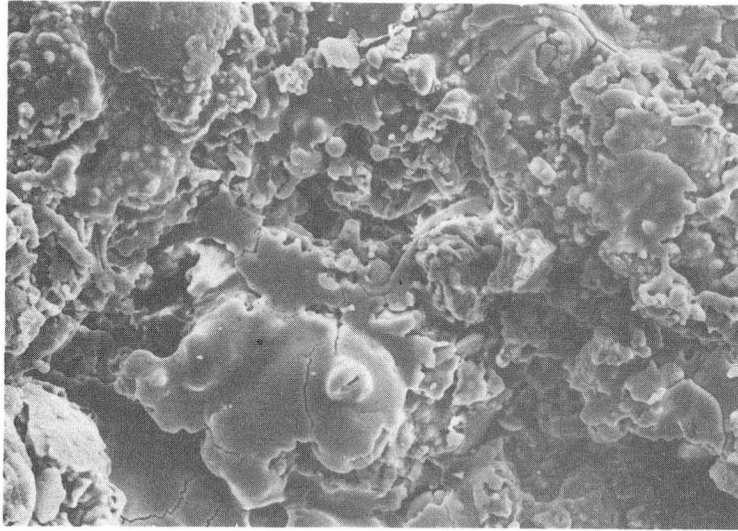
XBL 829-1131A



XBB 829-7744

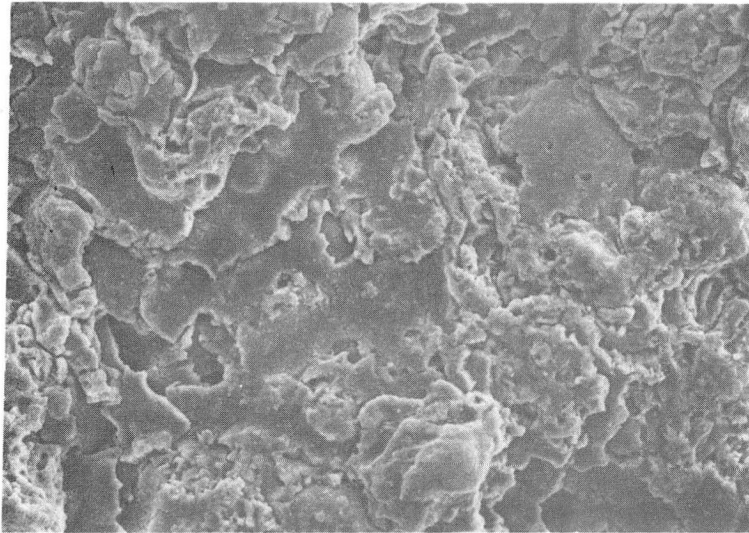
8 w/o YSZ 900 amp

Fig. 10. System no. 4 in the a) as-coated, b) eroded at 30° and c) eroded at 90° conditions



a

20 μ m



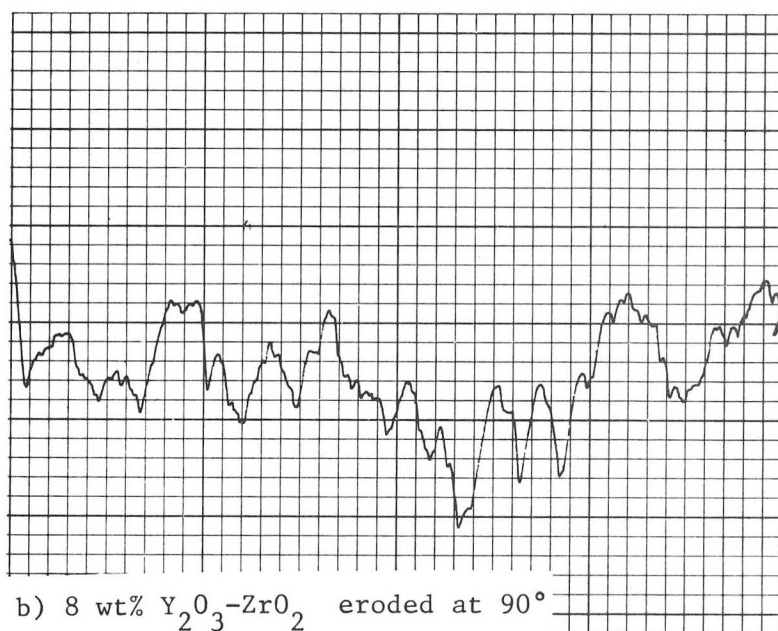
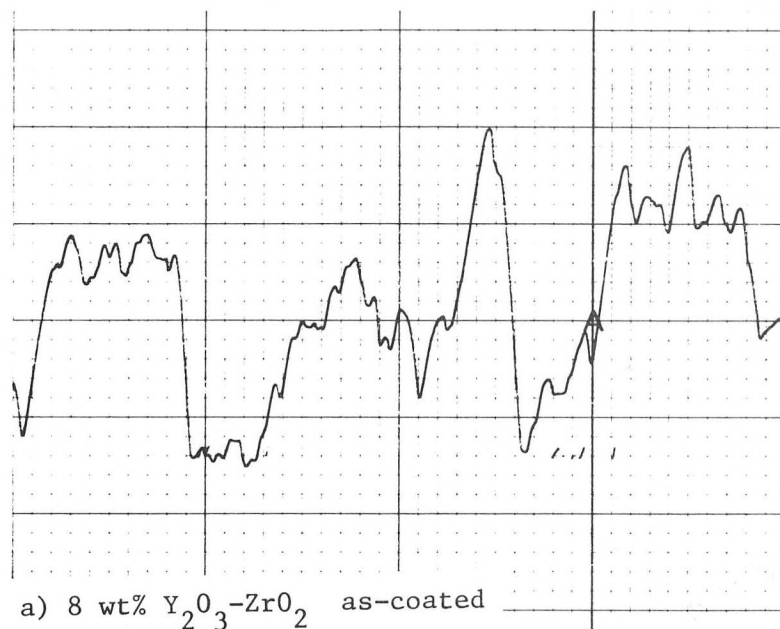
b

20 μ m

XBB 829-7743

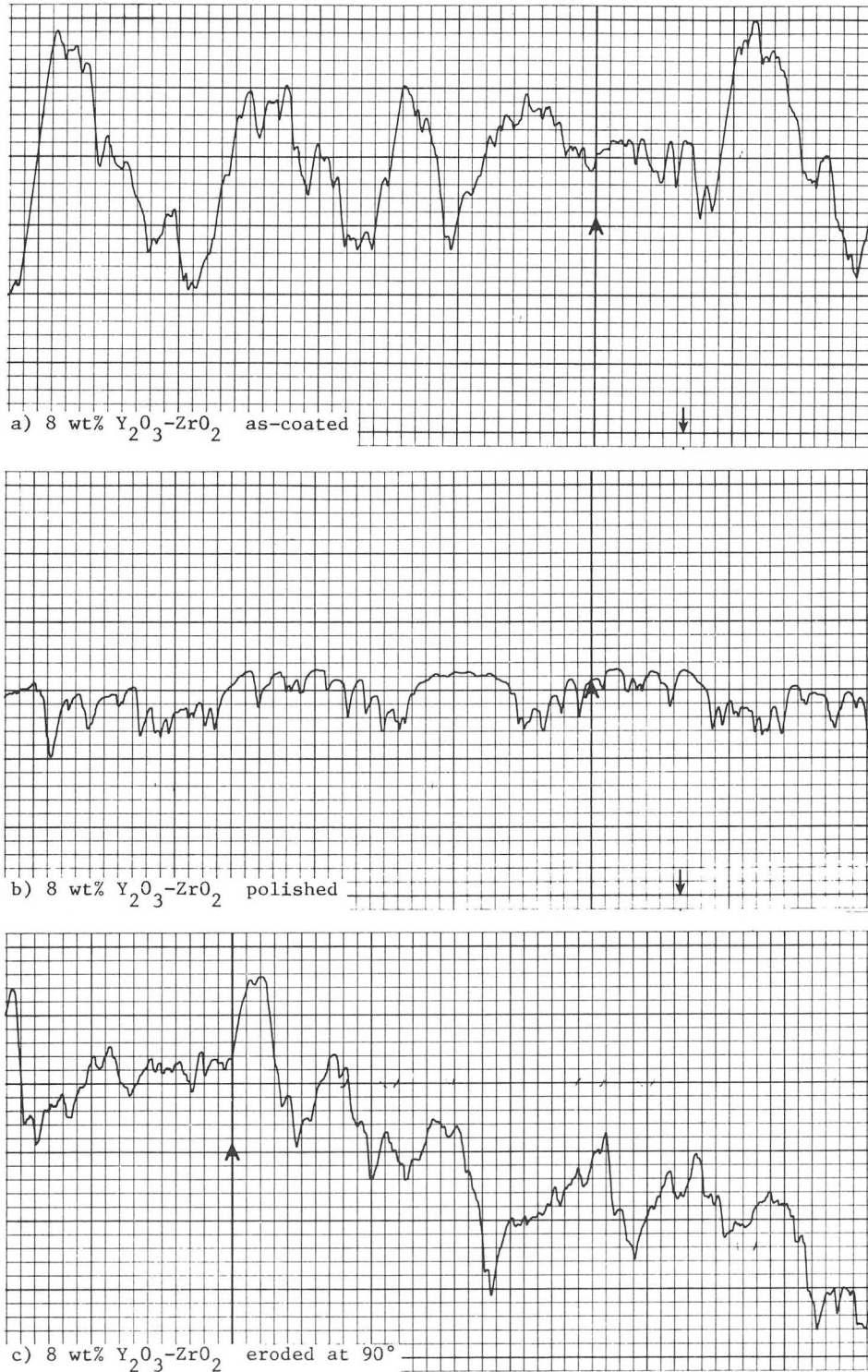
Fig. 11. System no. 6 in the a) as-deposited and b) eroded at 90° conditions

8 w/o YSZ



XBL 837-10504

Fig. 12. Surface profiles of system no. 6
 a) as-coated and b) after steady
 state erosion. Vertical scale:
 1 division = 200 micro-inches,
 chart speed 0.5 in/sec., traverse
 speed 0.01 in/sec.



XBL 837-10505

Fig. 13. Surface profiles of system no. 6. a) representative profile of the as-coated surface, b) system surface following a 5 minute polish with $1 \mu m$ alumina, c) profile of polished surface after erosion to the steady state condition. Vertical scale: 1 division = 200 micro-inches, chart speed .5 in/sec., traverse speed 0.01 in/sec.

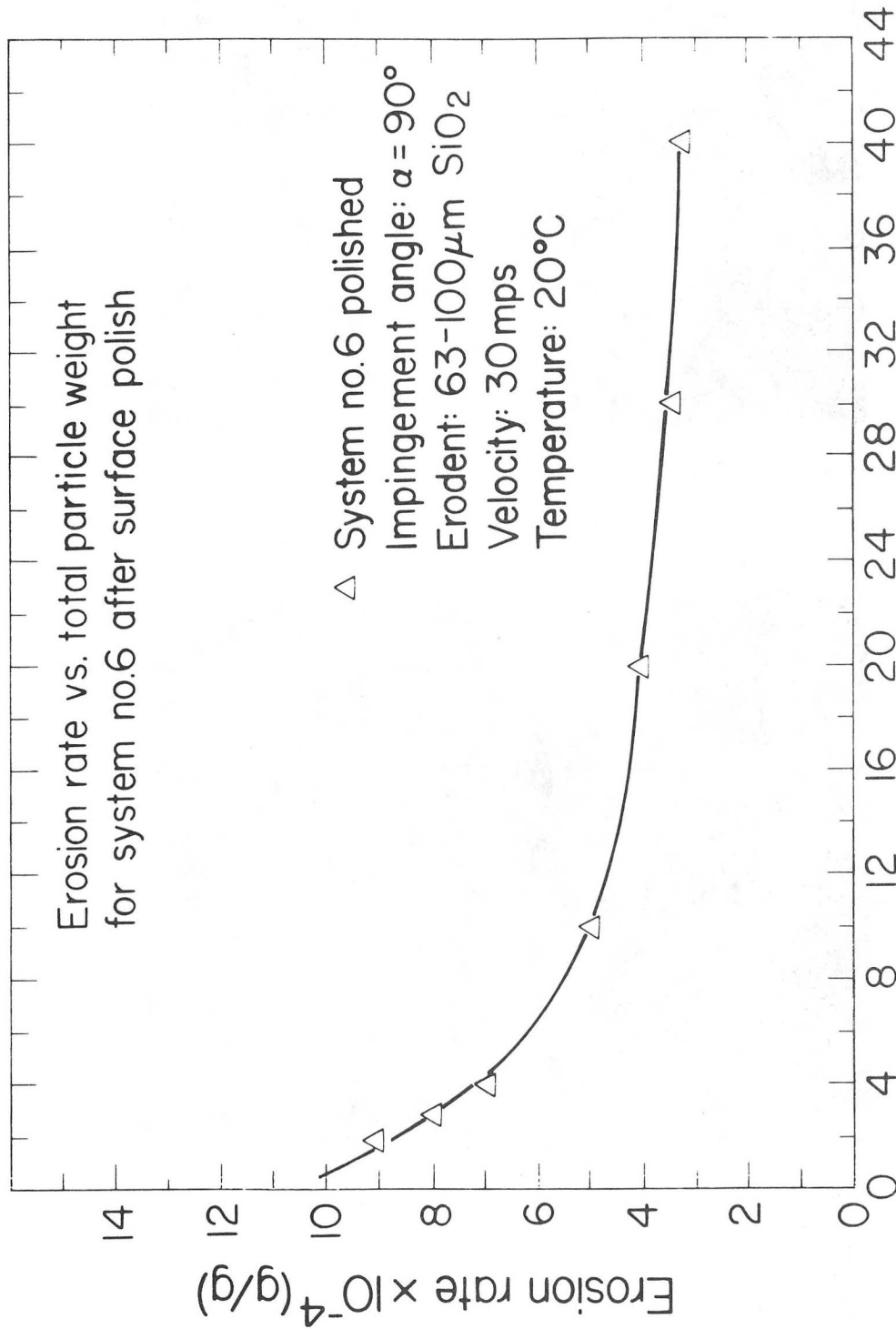
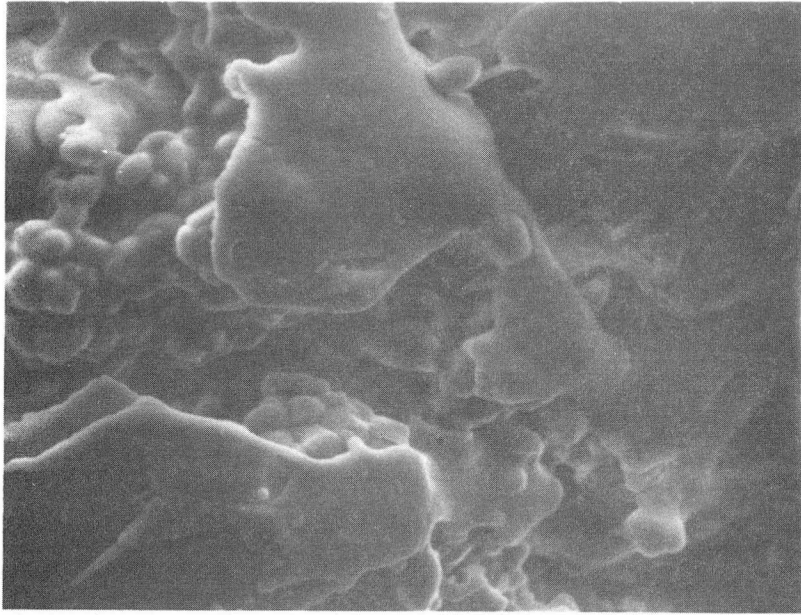


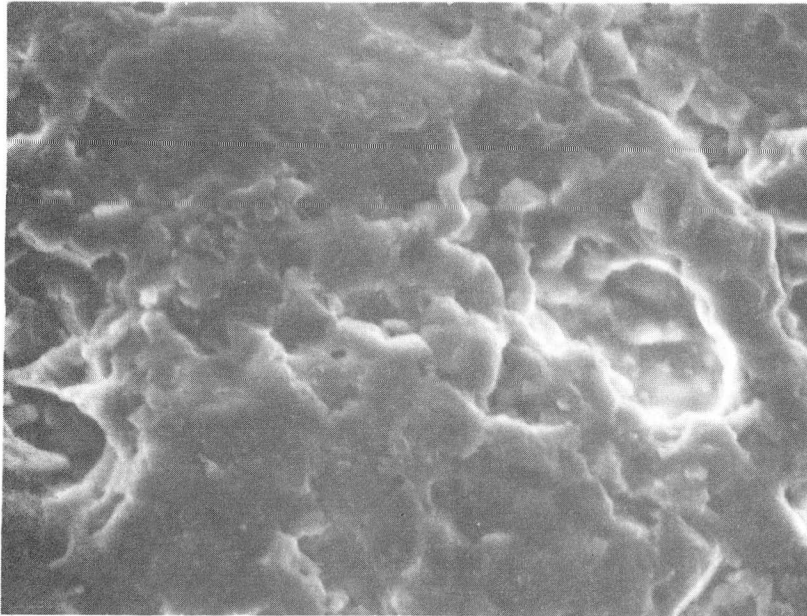
Fig. 14 Incremental erosion rate of system no. 6 after the as-coated surface was polished for 5 minutes with 1 μm Al₂O₃

XBL 8311-4600



a

5 μ m

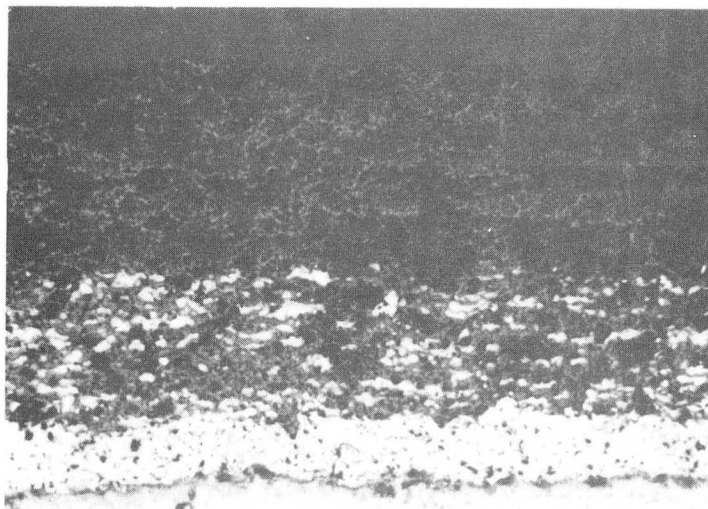


b

3 μ m

XBB 829-7745

Fig. 15. System no. 6 in the ^{8 w/o YSZ} a) as-coated and b) eroded at 90° conditions under high magnification



MgSZ

300 μm

XBB 829-7750

Fig. 16. Cross section of system no. 7 showing the mixed region of MgO-ZrO_2 and MCrAlY provided primarily for CTBC adherence enhancement

DISTRIBUTION LIST

Wate Bakker
EPRI
3214 Hillview Avenue
P.O. Box 10412
Palo Alto, CA 94304

B.R. Banerjee
Ingersoll-Rand Company
P.O. Box 301
Princeton, NJ 08540

K.L. Baumert
Air Products & Chemicals, Inc.
P.O. Box 538
Allentown, PA 18105

S.M. Benford
NASA Lewis Research Center
21000 Brookpark Road
Cleveland, OH 41135

A.E. Biggs
Arco Chemicals
3801 W. Chester Pike
Newtown Square, PA 19073

R. Blickensderfer
Bureau of Mines
P.O. Box 70
Albany, OR 97321

R.A. Bradley, Manager
Fossil Energy Materials Program
Oak Ridge National Laboratory
P.O. Box X
Oak Ridge, TN 37830

Richard Brown
Materials Laboratory
Department of Chemical Engineering
University of Rhode Island
Kingston, RI 02881

DISTRIBUTION LIST cont'd

D.H. Buckley
NASA Lewis Research Center
21000 Brookpark Road
Cleveland, OH 41135

P.T. Carlson, Task Leader
Fossil Energy Materials Program
Oak Ridge National Laboratory
P.O. Box X
Oak Ridge, TN 37830

J. Carpenter
ECUT Program
Oak Ridge National Laboratory
P.O. Box X
Oak Ridge, TN 37830

J.P. Carr
Department of Energy, Office of Fossil Energy
FE-42 Mailstop 3222-GTN
Washington, DC 40525

Hans Conrad
Materials Engineering Department
North Carolina State University
Raleigh, NC 27659

P. Crook
Cabot Corporation
Technology Department
1020 W. Park Avenue
Kokomo, IN 46901

S.J. Dapkunas
Department of Energy, Office of Fossil Energy
Technical Coordination Staff FE-14
Mailstop C-156 GTN
Washington, DC 40525

DOE Technical Information Center
P.O. Box 62
Oak Ridge, TN 37830

W.A. Ellingson
Argonne National Laboratory
9700 South Cass Avenue
Argonne, IL 60439

DISTRIBUTION LIST cont'd

J. Gonzales
GTE
Chemical & Metallurgical Division
Hawes Street
Towanda, PA 18848

Å. Hammarsten
Teknikum
P.O. Box 534, S-751 21
Uppsala
SWEDEN

E. Haycock
Westhollow Research Center
Shell Development Company
P.O. Box 1380
Houston, TX 77001

J.M. Hobday
Department of Energy
Morgantown Energy Technology Center
P.O. Box 880
Morgantown, WV 26505

E.E. Hoffman, Manager
National Materials Program
Department of Energy
Oak Ridge Operations
P.O. Box E
Oak Ridge, TN 37830

J.A.C. Humphrey
Mechanical Engineering Department
University of California
Berkeley, CA 94720

I.M. Hutchings
University of Cambridge
Department of Metallurgy
Pembroke Street
Cambridge
ENGLAND

Sven Jansson
Stal-Laval Turbin AB
Finspong S-61220
SWEDEN

DISTRIBUTION LIST cont'd

R.R. Judkins
Fossil Energy Materials Program
Oak Ridge National Laboratory
P.O. Box X
Oak Ridge, TN 37830

M.K. Keshavan
Union Carbide Corporation
Coating Services Department
1500 Polco Street
Indianapolis, IN 46224

T. Kosel
University of Notre Dame
Dept. of Metallurgical Engineering
& Materials Science
Box E
Notre Dame, IN 46556

L. Lanier
FMC-Central Engineering Laboratory
1185 Coleman Avenue
Santa Clara, CA 95052

N.H. MacMillan
Pennsylvania State University
167 Materials Research Laboratory
University Park, PA 16802

P.K. Mehrotra
Kennemetal Inc.
1011 Old Salem Road
Greensburg, PA 15601

Ken Magee
Bingham-Williamette Co.
2800 N.W. Front Avenue
Portland, OR 97219

T. Mitchell
Case Western Reserve University
Department of Metallurgy
Cleveland, OH 44106

Fred Pettit
Dept. of Metallurgy & Materials Engineering
University of Pittsburgh
Pittsburgh, PA 15261

DISTRIBUTION LIST cont'd

R.A. Rapp
Metallurgical Engineering
116 W. 19th Avenue
The Ohio State University
Columbus, OH 43210

D.A. Rigney
Metallurgical Engineering
116 W. 19th Avenue
The Ohio State University
Columbus, OH 43210

A.W. Ruff
Metallurgy Division
National Bureau of Standards
B-266 Materials
Washington, DC 20234

Alberto Sagüés
IMMR - University of Kentucky
763 Anderson Hall
Lexington, KY 40506

Gordon Sargent
University of Notre Dame
Dept. of Metallurgical Engineering & Materials Science
Box E
Notre Dame, IN 46556

Paul Shewmon
Dept. of Metallurgical Engineering
116 W. 19th Avenue
Columbus, OH 43210

Gerry Sorell
EXXON Research & Engineering Company
P.O. Box 101
Florham Park, NJ 07932

John Stringer
University of California
Lawrence Berkeley Laboratory
Mailstop 62/203
Berkeley, CA 94720

Widen Tabakoff
Dept. of Aerospace Engineering
University of Cincinnati
Cincinnati, OH 45221

DISTRIBUTION LIST cont'd

Edward Vesely
IITRI
10 West 35th Street
Chicato, IL 60616

J.J. Wert
Metallurgy Department
Vanderbilt University
P.O. Box 1621, Sta. B
Nashville, TN 37235

J.C. Williams
Dept. of Metallurgy & Materials Science
Carnegie-Mellon University
Schenley Park
Pittsburgh, PA 15213

S. Wolf
Department of Energy
Basic Energy Sciences Office
Division of Materials Sciences
Washington, DC 20545

Ian Wright
Materials Science Division
Battelle Memorial Institute
505 King Avenue
Columbus, OH 43201

C.S. Yust
Metals and Ceramics Division
Oak Ridge National Laboratory
P.O. Box X
Oak Ridge, TN 37830

This report was done with support from the Department of Energy. Any conclusions or opinions expressed in this report represent solely those of the author(s) and not necessarily those of The Regents of the University of California, the Lawrence Berkeley Laboratory or the Department of Energy.

Reference to a company or product name does not imply approval or recommendation of the product by the University of California or the U.S. Department of Energy to the exclusion of others that may be suitable.

TECHNICAL INFORMATION DEPARTMENT
LAWRENCE BERKELEY LABORATORY
UNIVERSITY OF CALIFORNIA
BERKELEY, CALIFORNIA 94720